Modeling the Phase Behavior of the Inverse Hexagonal and Inverse Bicontinuous Cubic Phases in 2:1 Fatty Acid/Phosphatidylcholine Mixtures

R. H. Templer,* J. M. Seddon, and P. M. Duesing

Department of Chemistry, Imperial College, London SW7 2AY, U.K.

R. Winter and J. Erbes

University of Dortmund, Department of Chemistry, Physical Chemistry I, D-44221 Dortmund, Germany

Received: August 29, 1997; In Final Form: November 13, 1997

In this paper we present simplified models of the energetics of the inverse hexagonal (H_{II}) and inverse bicontinuous cubic phases (Q_{II}^{P}, Q_{II}^{D}, and Q_{II}^{G}) based upon the competition between the energetics of monolayer bending and the packing of amphiphiles within each mesophase. These are used to interpret our experimental observations of the relative stability of these mesophases in 2:1 (mol:mol) fatty acid/phosphatidylcholine mixtures (Templer, R.H.; Seddon, J.M.; Warrender, N.A.; Syrykh, A.; Huang, Z.; Winter, R.; Erbes, J. *J. Phys. Chem.*, submitted for publication). We have used our models to rationalize the following observations made at atmospheric pressure: the phase sequences with water composition, the destabilization of the inverse bicontinuous cubics with increasing chain lengths and temperature, and the phase transition from Q_{II}^{P} to Q_{II}^{D} with increasing temperature. We show, for the first time, that phase transitions between the inverse bicontinuous cubic phases may be explained in terms of a change in their interfacial geometry. Data from the C_{12} mixtures indicates that the preferred radius of curvature of the system decreases by 0.09 Å $°C^{-1}$ and that the ratio of the rigidity for coupled mode bending to the bare bending rigidity is 0.14. The latter lies in the range predicted by theory (Templer, R. H.; Khoo, B. J; Seddon, J. M. *Langmuir*, in preparation).

1. Introduction

We have previously presented experimental results on the phase and structural behaviour of 2:1 (mol/mol) mixtures of fatty acids and phosphatidylcholines in water.[1,2] These results have been for a homologous series beginning at the C_{12} chain length and ending at C_{18}. In this paper we are concerned with modelling our observations of the phase behavior of the inverse hexagonal (H_{II}, Figure 1a) phase and inverse bicontinous cubic phases (Q_{II}^{P}, Q_{II}^{D}, and Q_{II}^{G}, Figures 1b−d) in the C_{12} and C_{14} mixtures: lauric acid and 1,2-dilauroyl-*sn*-glycero-3-phosphocholine (LA/DLPC) and myristic acid and 1,2-dimyristoyl-*sn*-glycero-3-phosphocholine (MA/DMPC), respectively.

There are three rather general features of the competition between the inverse hexagonal and inverse bicontinuous cubic phases which we wish to model. (i) In systems where all are present (2:1 LA/DLPC), the phases appear in the order $H_{II} \rightarrow Q_{II}^{G} \rightarrow Q_{II}^{D} \rightarrow Q_{II}^{P}$ with increasing water content, Figure 2a. (ii) In such systems increasing the temperature destabilizes Q_{II}^{P} with respect to Q_{II}^{D} and the H_{II} phase. (iii) Increasing the lipid chain length destabilizes all the inverse bicontinuous cubic phases with respect to the H_{II} phase. In this homologous series, this begins with 2:1 MA/DMPC where there is coexistence in excess water between Q_{II}^{P} and the H_{II} phase, Figure 2b, but at the longer chain lengths the cubic phases disappear completely.[2]

We will attempt to model these observations in terms of a competition between the lipid monolayer's desire to bend isotropically and the packing and bending frustration that ensues because of the fixed Euclidean geometries into which the monolayer must be embedded.[3] We are not, as yet, able to include free energy contributions for the van der Waals attraction between bilayers nor the hydration and fluctuational repulsions between them. For this reason the lamellar phase must be excluded from our theoretical interpretations. Our discussions are structured in the following manner. Section 2 deals with the mathematical basis of our models, first introducing the essential elements of our energetic theory, before presenting specific models of each phase. Section 3 uses these models to fit the experimental data and provide a basis for interpreting the physical origins of our observations. We conclude with a summary of the strengths and weaknesses of our modeling and point to possible future advances in understanding the inverse bicontinuous cubic phases.

2. Energetic Theory

Before we deal with the specifics of the bending energy and packing frustration models for the H_{II}, Q_{II}^{P}, Q_{II}^{D}, and Q_{II}^{G} phases we introduce the curvature elastic free energy per molecule in the monolayer,[4] outline how we will deal with packing frustrations, and describe the limitations of our modeling.

The curvature elastic energetics will be modeled in terms of the departures away from the completely relaxed monolayer state. Since the amphiphiles in the monolayer form a two dimensional fluid, the torque tension in the monolayer should be isotropic. Hence, when we remove all geometrical packing frustration, the resulting monolayer should be spherical and therefore we need define only one curvature for this relaxed state c_r. This assumption is identical to that used in the well-known Helfrich ansatz.[5] Furthermore, we have experimentally

S1089-5647(97)02837-X CCC: $15.00
Published on Web 02/11/1998

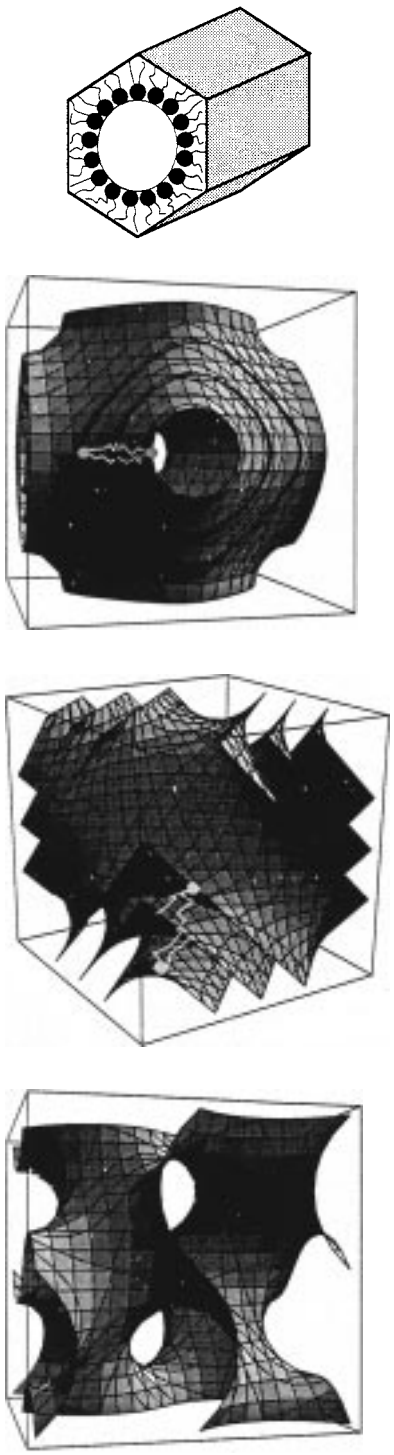

Figure 1. The inverse phases in 2:1 FA/PC mixtures. From top to bottom, the unit cells of (a) the inverse hexagonal H_{II} phase, (b) the P cubic, space group *Im*3*m*, symbol Q_{II}^{P}, (c) the D cubic, space group *Pn*3*m*, symbol Q_{II}^{D} and (d) the G cubic, space group *Ia*3*d*, symbol Q_{II}^{G} are illustrated. In a−c the location of the amphiphiles is shown. For reasons of clarity we have only shown the bilayer midplane for Q_{II}^{G}.

confirmed this assumption in the case of 1-monoolein, where the addition of long-chain alkane leads to a completely packing stress relieved monolayer state which is spherical.[6] For a monolayer of arbitrary shape the principal curvatures are c_1 and c_2 and hence the departures from equilibrium are $\Delta c_1 = c_1 - c_r$ and $\Delta c_2 = c_2 - c_r$. We will define the sign of the curvature to be negative if the curvature is toward the aqueous component.

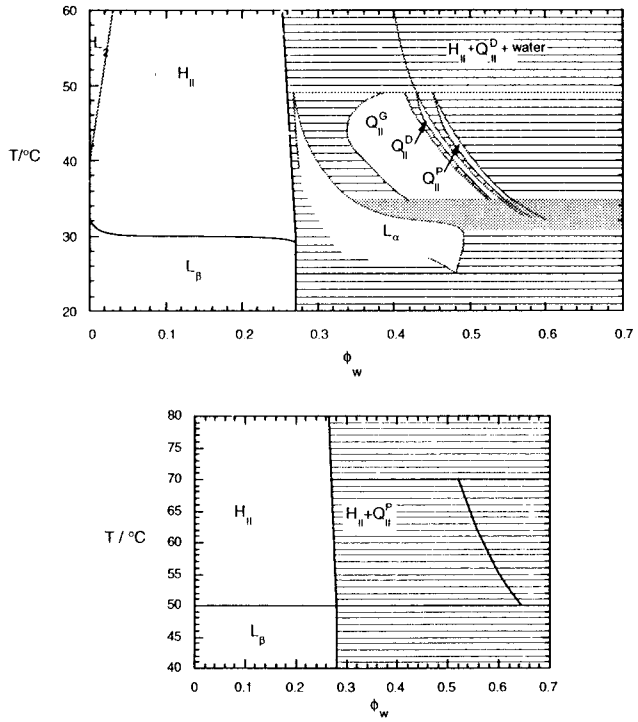

Figure 2. From top to bottom: (a) the phase diagram for 2:1 (mol:mol) LA/DLPC at atmospheric pressure. Those phase boundaries which are the least well characterized are shown in grey and the region between the L_α, L_β, and H_{II} phases has not been completely characterized. (b) The phase diagram for 2:1 (mol:mol) MA/DMPC at atmospheric pressure. There is some evidence of metastable bicontinuous phases of space group *Ia*3*d* and *Pn*3*m* in the coexistence region $H_{II} + Q_{II}^{P}$.

An expansion up to quadratic terms in Δc_1 and Δc_2 for the curvature elastic energy per unit area g_c can then be expressed as

$$g_c = {}^1/_2 k \Delta c_1^2 + {}^1/_2 k \Delta c_2^2 + \bar{k} \Delta c_1 \Delta c_2 \qquad (1)$$

where k is the bare bending rigidity and $\bar{k}$ is the rigidity for coupled mode bending. It can be shown that for mechanical stability $k \geq \bar{k} \geq 0$. We will make our measurements of curvature at the area neutral or pivotal surface[7] (that position on the molecule whose area is constant for bending at constant temperature and pressure). The molecular cross section at the pivotal surface is A_n, so we may find the free energy per molecule by multiplying (1) by this value. Furthermore we note that we can divide the result by the bending rigidity to give us a unitless free energy per molecule for monolayer curvature, $\bar{\mu}_c$

$$\bar{\mu}_c = A_n\left[{}^1/_2 \Delta c_1^2 + {}^1/_2 \Delta c_2^2 + \frac{\bar{k}}{k} \Delta c_1 \Delta c_2\right] \qquad (2)$$

It will be helpful to reexpress (2) in terms of the mean curvature at the pivotal surface, $H_n = {}^1/_2(c_1 + c_2)$, and the Gaussian curvature there, $K_n = c_1 c_2$,

$$\bar{\mu}_c = A_n\left[\left(1 + \frac{\bar{k}}{k}\right)(H_n - H_r)^2 + \left(1 - \frac{\bar{k}}{k}\right)(H_n^2 - K_n)\right] \qquad (3)$$

where $H_r = c_r$ is the preferred mean curvature at the pivotal surface.

We can immediately see from (3) that the free energy per molecule associated with bending the interface will always be greater for the inverse bicontinuous cubics than that for the

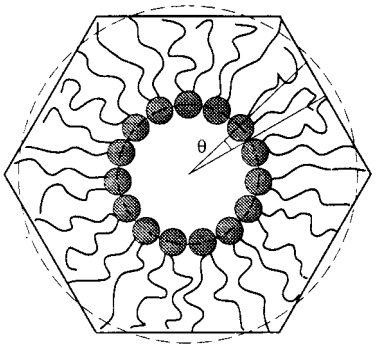

Figure 3. Frustration in the inverse hexagonal phase. We show a perpendicular cross section through the unit cell. For a uniform cylindrical interface the average location of the terminal methyl groups would also be cylindrical, as shown by the outer dotted line, but the unit cell geometry forces monolayer extension around $\theta = (2n + 1)\pi/6$ and compression around $\theta = n\pi/3$.

inverse hexagonal geometry as long as $k \geq \bar{k} \geq 0$. This is so, because $K_n = 0$ for the H_{II} phase, but is negative for the bicontinuous cubics, making the second term in (3) greater for the hyperbolic interfaces at any value of H_n. So if we are to stabilize the inverse bicontinuous cubic phases relative to the H_{II} phase, an additional free energy will be needed: the amphiphile packing frustration.

It is rather straightforward to show how this arises in the H_{II} phase, Figure 3. Here, if we constrain the pivotal surface to lie on a cylinder (i.e. to have uniform curvature) it is clear that chains will be in compression close to $\theta = n\pi/3$ and in extension around $\theta = (2n + 1)\pi/6$ ($n = 0, 1, 2, 3$, etc.). In fact one would imagine that the system would simultaneously allow variations in interfacial curvature, interfacial area, and chain extension in order to minimize the total free energy per molecule. Indeed, experimental data on the H_{II} phase indicates that this is probably the case.[8] However, the mathematical solution to this problem is extremely complex and our attempts at finding a viable approach are in their infancy.[9] We have therefore followed the expedient of defining the shape of the interface first, and then determining the energetics, rather than allowing the energetics to set the shape.

This is the approach that everyone to date has followed. In most cases it seems that this produces models capable of giving us important semiquantitative insights into the workings of lyotropic mesophase energetics. However, in the case of the inverse bicontinuous cubic phases, there has been a significant stumbling block. In most cases these phases have been modeled by assuming that the interface is a constant distance from the underlying minimal surface.[10−14] This is mathematically convenient, but gives us the result that the three bicontinuous cubic phases Q_{II}^P, Q_{II}^D, and Q_{II}^G are energetically degenerate.[15] Except where these phases are highly swollen, all our experimental work suggests that this is not in fact the case.[1] We will show that this is in fact a consequence of our choice of interface geometry. By changing the geometry we can break the degeneracy and hence gain some qualitative understanding of the phase transitions between inverse bicontinuous cubic phases.

From the above it should be clear that the detailed models which follow contain significant simplifications to make our calculations tractable. As we have already stated, we will set the geometry of the pivotal surface. We will quantify only the bending energy and the packing energy in each phase at this surface. This means we have ignored any interactions between monolayers; the van der Waals attraction, hydration repulsion, and fluctuation repulsions (our system is zwitterionic so we need not consider electrostatic repulsions). For systems such as the FA/PC mixtures, the bending rigidity of the interface is thought to be great enough that these other energetic terms are of secondary significance to the stability of the nonlamellar phases. We are not basing our modeling of the bending energetics on the more formally correct neutral surface, where interfacial bending and interfacial stretching are decoupled, for a number of reasons. Firstly, this approach makes the theoretical treatment of hyperbolic interfaces extremely complex. Secondly, our fitting of the swelling data for the 2:1 FA/PC mixtures in the first paper in this series indicated that there was little or no interfacial stretching at the pivotal surface during bending. In general it is true that this does not necessarily mean that there has been no interfacial stretching at the pivotal surface,[16] Figure 4, but it would be exceptionally fortuitous for the bending deformations to mask interfacial stretching over the wide range of interfacial curvatures we have recorded.[1]

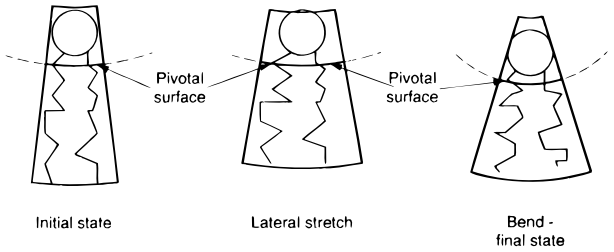

Figure 4. The pivotal surface does not necessarily decouple bending and stretching modes. We decompose the molecular deformation between an initial and final state into two separate steps: a stretch and a bend. This shows that we can stretch the interface at the pivotal surface, but then counteract this dilation in the bending deformation. The net effect is that we see no change in area at the pivotal surface, but the bending and stretching modes are not decoupled.

2.1. Inverse Hexagonal Phase. For the inverse hexagonal phase the simplest geometrical choice is to make the interface cylindrical. Then the surface average of the curvature elastic free energy per molecule, $\langle \bar{u}_c \rangle$ is simply

$$\langle \bar{u}_c \rangle = A_n\left[\left(1 + \frac{\bar{k}}{k}\right)(H_n - H_r)^2 + \left(1 - \frac{\bar{k}}{k}\right)H_n^2\right] \qquad (4)$$

H_n being uniform and $\langle ... \rangle$ indicating a surface average.

We have already shown that such a cylindrical interface embedded in the H_{II} geometry suffers a physical frustration due to the variation in the distance between the pivotal surface and the edge of the unit cell. Thickening or thinning a curved interface while maintaining a uniform monolayer density cannot be done without an accompanying change in either the molecular splay of the amphiphiles, their cross-sectional area, or both. In order to keep the number of adjustable parameters in our description to a minimum we choose to model the variation in monolayer thickness in terms of molecular splay. This is done by setting the area per molecule at the pivotal surface and the molecular volume between this and the edges of the unit cell to be constant. The frustration energy will then be quantified by determing the splay (mean curvature) the molecule would need at any point on the interface to reach the unit cell boundary, Figure 5.

Our estimate of the frustration energy is then equal to the curvature elastic cost of mean curvature deviations away from H_n. The unitless frustration energy per molecule $\langle \bar{u}_f \rangle$ will then be given by

$$\langle \bar{u}_f \rangle = A_n\left[\left(1 + \frac{\bar{k}}{k}\right)\langle (H_c - H_n)^2 \rangle + \left(1 - \frac{\bar{k}}{k}\right)\langle H_n^2 \rangle\right] \qquad (5)$$

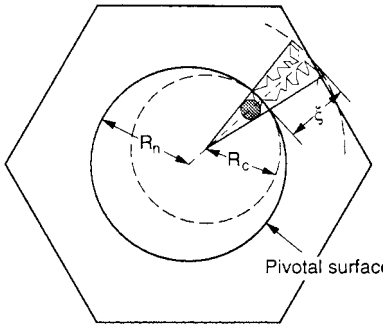

Figure 5. The frustration tied up in stretching or compressing lipid chains between the pivotal surface and the edges of the unit cell can be modeled as a change in molecular splay. The molecule is compressed to a length ξ so it just touches the unit cell edge by increasing its splay, so that the radius of curvature of the molecule is now $R_c = -1/2H_c$ (see main text) rather than $R_n = -1/2H_n$.

where H_c is the molecular mean curvature that is required to achieve the required chain extension.

To determine the surface averages of H_c, we need the relationship between the perpendicular distance from the pivotal surface to the chain ends ξ and H_c. First we recall that the molecular area at the pivotal surface A_n is constant and that the molecular volume between this surface and the edges of the unit cell ν_n is also constant. We may then use the differential geometry of a monolayer with cylindrical curvature to relate to ξ to H_c

$$H_c = \frac{\xi - (\nu_n/A_n)}{\xi^2} \tag{6}$$

The variation in ξ (and hence H_c) is found from the geometrical relationship

$$\xi = \frac{a}{2\cos\theta} - R_n \tag{7}$$

where a is the lattice parameter of the H_{II} phase, the angle θ is as defined in Figure 3, and R_n is the radius of the pivotal surface (equal to $-H_n/2$). Since R_n and a are fixed at a given water volume fraction, ϕ_w, we may now determine $\langle\bar{u}_f\rangle$

$$\langle\bar{u}_f\rangle = A_n\left[\frac{1}{\pi}\int_0^{2\pi}\left(\frac{1}{\xi} - \frac{\nu_n}{A_n\xi^2}\right)^2 d\theta - \frac{(1+\bar{k}/k)H_n}{\pi}\int_0^{2\pi}\left(\frac{1}{\xi} - \frac{\nu_n}{A_n\xi^2}\right)d\theta + (1+\bar{k}/k)H_n^2\right] \tag{8}$$

To model the experimental data we express $\langle\bar{u}_c\rangle + \langle\bar{u}_f\rangle$ in terms of ϕ_w, using expressions for R_n and a as a function of ϕ_w previously derived.[1]

2.2. Inverse Bicontinuous Cubic Phases: Parallel Interface. We now turn to our determination of the energetics of the bicontinuous cubic phases. Here we have two mathematically tractable options for our choice of interfacial geometry: an interface which lies at a constant distance away from the underlying minimal surface, the parallel surface model,[10] or one in which the interface projected away from the underlying minimal surface has constant, but nonzero mean curvature.[17,18] We will deal with the parallel surface model first.

Unlike our model for the H_{II} phase in which H_n was homogeneous, if we model the bicontinuous cubic phases with interfaces, which are parallel to the underlying minimal surface, both H_n and K_n will be inhomogeneous. The surface average of the curvature elastic energy per molecule therefore requires a calculation of the surface averages of the mean and Gaussian curvature at the neutral surface

$$\langle\bar{u}_c\rangle = A_n\left[\left(1+\frac{\bar{k}}{k}\right)\langle(H_n - H_r)^2\rangle + \left(1-\frac{\bar{k}}{k}\right)(\langle H_n^2\rangle - \langle K_n\rangle)\right] \tag{9}$$

It has been shown[14] that this is given by

$$\langle\bar{u}_c\rangle = A_n\left[\left(1+\frac{\bar{k}}{k}\right)H_r^2 + \sum_{p=1}^{\infty}\left[\frac{1}{\xi^2}\left\{\left(1-\frac{\bar{k}}{k}\right) + 2\left(1+\frac{\bar{k}}{k}\right)H_r\xi + 2\sum_{m=2}^{p(p>1)} f_m\right\}\left\{\frac{\langle\nu_n\rangle - \langle A_n\rangle\xi}{\langle\nu_n\rangle - \langle A_n\rangle\xi/3}\right\}^p\right]\right] \tag{10}$$

where we have used the substitution[14]

$$\langle K\rangle = [\langle A_n\rangle\xi - \langle\nu_n\rangle]/[\xi^2(\langle\nu_n\rangle - \langle A_n\rangle\xi/3)] \tag{11}$$

and $f_m = \langle K^m\rangle/\langle K\rangle^m$. The first eight values of f_m are $f_1 = 1$ (which does not appear in this expansion), $f_2 = 1.21872$, $f_3 = 1.60678$, $f_4 = 2.21644$, $f_5 = 3.15380$, $f_6 = 4.59516$, $f_7 = 6.82347$, and $f_8 = 10.2938$ and these terms arise because of the inhomogeneity of the mean and Gaussian curvature at the interface. When the cubic lattice is rather large (more precisely when $|\langle K\rangle|\xi^2 \ll 1$) the magnitude of the inhomogeneity is small and only the first term in the expansion is needed to adequately describe the energetics. As the size of the bicontinuous cubic phase shrinks, the inhomogeneity becomes increasingly important and this is reflected in the increase in the relative magnitude of the inner summation. Since in these cases there are sizeable variations in the interfacial curvature, it is possible that the first-order bending moduli might be insufficient to accurately model the bending energetics in these phases. However, given the semiquantitative nature of the researches reported here, and in an effort to keep the number of fitting parameters to a minimum we have decided to assume that additional curvature elastic moduli are not needed.

The physical frustration which arises out of the parallel surface geometry is due to the variation in molecular geometry imparted by the inhomogeneous curvature of the minimal surface. The molecular area at the pivotal surface is given by $A_n = A_u(1 + K\xi^2)$, where A_u is the molecular area at the minimal surface, the pivotal surface volume is given by $\nu_n = A_u\xi(1 + K\xi^2/3)$ and the molecular volume by $\nu = A_u l(1 + Kl^2/3)$, where l is the monolayer thickness.[10] Using these relations, one can show that $\langle\nu_n\rangle/\langle\nu\rangle \neq \langle\nu_n/\nu\rangle$ and $\langle A_n\rangle/\langle\nu\rangle \neq \langle A_n/\nu\rangle$ which means that ν, ν_n, nor A_n can be homogeneous (although the inhomogeneity becomes vanishingly small as the magnitude of K becomes small).

In order to factor out variations in A_n and describe the frustration in terms of quantities relevant to the pivotal surface from which the curvature elastic measurements are to be made, we have decided to model the geometrical frustration energy per molecule $\langle\bar{u}_f\rangle$ in terms of the variance in the molecular shape parameter $i = \nu_n/A_n\xi$ about the surface-averaged value

$$\langle\bar{u}_f\rangle = \frac{\langle A_n\rangle\eta}{2k}\left(\frac{\langle i^2\rangle}{\langle i\rangle^2} - 1\right) \tag{12}$$

where η is the modulus associated with variations in i. To put (12) into a usable form, we substitute for ν_n and A_n in i, using the expressions given in the previous paragraph, and then determine surface averages after expansion. Using (11) we

substitute for the surface average of the Gaussian curvature to obtain an expression, similar to (10), which is entirely in terms of ξ

$$\langle \bar{u}_f \rangle = \frac{\langle A_n \rangle \eta}{2k} \times$$

$$\left\{ \frac{1 + 4\left(\frac{\langle \nu_n \rangle - \langle A_n \rangle \xi}{3\langle \nu_n \rangle - \langle A_n \rangle \xi}\right) + \sum_{m=2}^{\infty} \frac{4m-1}{2} f_m \left(\frac{\langle \nu_n \rangle - \langle A_n \rangle \xi}{\langle \nu_n \rangle - \langle A_n \rangle \xi/3}\right)^m}{\left[1 + {}^2/_3 \sum_{m=1}^{\infty} f_m \left(\frac{\langle \nu_n \rangle - \langle A_n \rangle \xi}{\langle \nu_n \rangle - \langle A_n \rangle \xi/3}\right)^m\right]^2} - 1 \right\} \quad (13)$$

In order to express the total energy as a function of the water volume fraction, we use the relationships between ξ and ϕ_w previously derived.[1]

2.3. General Observations: Part I. Inspection of the models confirms that, in the absence of any other free energy terms, the curvature elastic energy of the H_{II} phase is always less than that of the inverse bicontinuous cubics, Figure 6a. The difference in the curvature elastic free energy cost between the phases decreases as the magnitude of H_r decreases or $\bar{k}/k$ tends to unity. In general, however, we would anticipate that it is the frustration energy which might act to stabilize the bicontinuous phases, under the appropriate conditions.

The frustration energy in the H_{II} phase rises as we increase the water volume fraction, whereas the frustration energy in the bicontinuous cubics, with parallel interface geometry, becomes vanishingly small at high water fractions, Figure 6b. Hence one would expect to find the bicontinuous cubic phases on the high water content side of the inverse hexagonal phase, Figure 6c. Furthermore, one would expect them to be destabilized by one or other of three factors: an increase in the magnitude of H_r, an increase in the value of η/k, or a decrease of $\bar{k}/k$ to values close to zero. Because of their space filling properties, one finds that the inverse bicontinuous cubic phases themselves should always appear in the sequence $Q_{II}^G \rightarrow Q_{II}^D \rightarrow Q_{II}^P$ as one increases the water content,[15] Figure 6.

While we will go on to show that the parallel interface geometry for the bicontinuous cubics is an extremely useful model for interpreting the phase diagrams of 2:1 FA/PC mixtures, the reader should note that the model has resulted in a rather disconcerting energetic degeneracy between the three cubic phases. This energetic degeneracy is in fact not observed in our experimental results, except perhaps where the inverse bicontinuous cubic phases are extremely hydrated. We now go on to show that, with an interfacial geometry other than the parallel surface, one can break the degeneracy of the mathematical model.

2.4. Inverse Bicontinuous Cubic Phases: Constant Mean Curvature Interface. The geometry of interfaces with constant mean curvature for Q_{II}^P, Q_{II}^D, and Q_{II}^G have recently been determined.[17,18] For such an interface the surface averaged curvature elastic energy is given by

$$\langle \bar{u}_c \rangle = A_n \left[\left(1 + \frac{\bar{k}}{k}\right)(H_n - H_r)^2 + \left(1 - \frac{\bar{k}}{k}\right)(H_n^2 - \langle K_n \rangle) \right] \quad (14)$$

where H_n and $\langle K_n \rangle$ must be determined as a function of the water volume fraction for Q_{II}^P, Q_{II}^D, and Q_{II}^G using the computations of Anderson and Grosse-Brauckmann.[17,18]

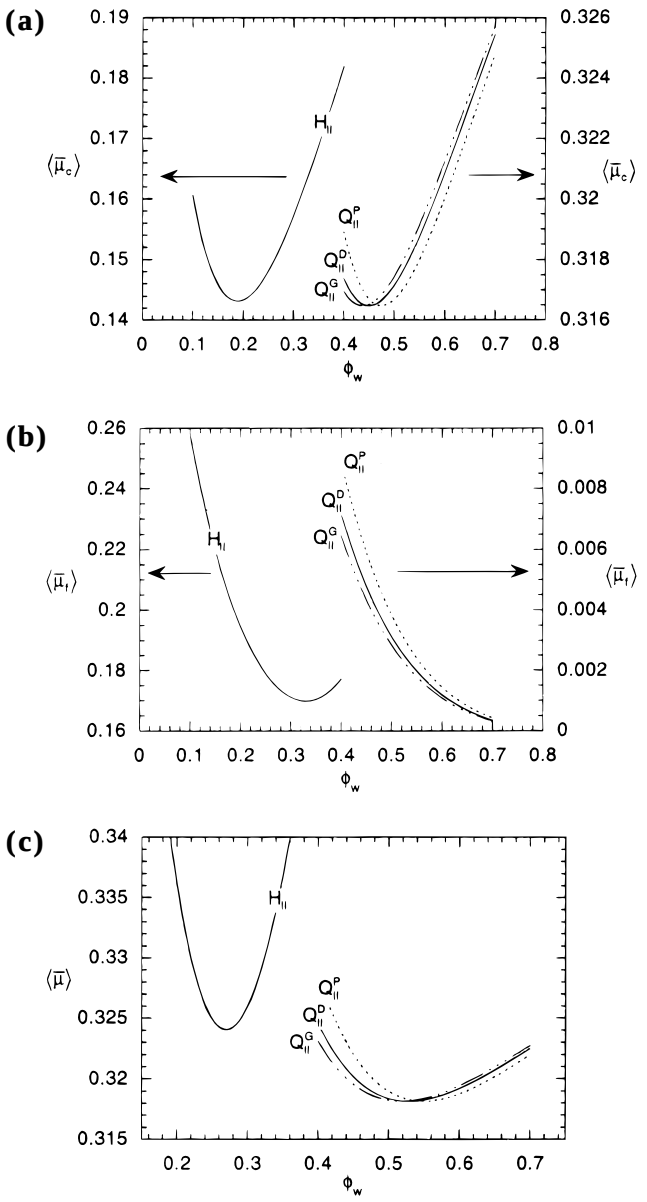

Figure 6. (a) The calculated curvature elastic energy per molecule, (b) frustration energy per molecule, and (c) total energy per molecule as a function of water volume fraction in the H_{II} and inverse bicontinuous cubic phases (note the differences in energy scale). The calculations have been made for $A_n = 108$ Å^2, $\nu_n = 1230$ Å^3, $\nu = 1736$ Å^3, $\bar{k}/k = 0.14$, $H_r = -0.052$ Å^{-1}, and $\eta/k = 0.07$ Å^{-2}.

Let us deal with the surface-averaged Gaussian curvature first. According to the Gauss−Bonnet theorem the surface-averaged Gaussian curvature is given by

$$\langle K_n \rangle = \frac{2\pi\chi}{S_n} \quad (15)$$

where S_n is the surface area at the pivotal surface for one monolayer within the unit cell. The dimensionless surface areas of interfaces (area divided by lattice parameter squared) with constant mean curvature have been computed at various volume fractions. We have fitted the computed values for Q_{II}^P, Q_{II}^D, and Q_{II}^G using a series in even powers of the volume fraction of the pivotal surface $\phi_n = \nu_n/\nu(1-\phi_w)$ to obtain

$$S_n = a^2 \sum_{i=0} \sigma_i \phi_n^{2i} \quad (16)$$

where the coefficients, σ_i, are shown in Table 1.

TABLE 1: Coefficients to Calculate the Gaussian Curvature of the Constant Mean Curvature Inverse Bicontinuous Cubic Phases[a]

	Q_{II}^G	Q_{II}^D	Q_{II}^P
σ_0	3.0915	1.9189	2.3451
σ_1	−1.3317	−0.8893	−1.1713
σ_2	−0.19974	−0.061856	−0.22227
σ_3	−0.80113	−0.65474	−2.4952
useable range	$0 < \phi_n < 0.888$	$0 < \phi_n < 0.738$	$0 < \phi_n < 0.500$
maximum error	<0.4%	<0.1%	<0.3%

[a] Upper limit to the useable range is the maximum possible neutral surface volume fraction for each phase. The error quoted is the maximum error between the fitted and computed values of the Gaussian curvature.

TABLE 2: Coefficients to Calculate the Mean Curvature of the Constant Mean Curvature Inverse Bicontinuous Cubic Phases[a]

	Q_{II}^G	Q_{II}^D	Q_{II}^P
ς_0	2.7953	1.8379	3.0458
ς_1	−9.9778	−0.17345	−14.256
ς_2	59.478	16.508	237.3
ς_3	−111.96	−62.547	−1365.6
ς_4	74.685	76.638	2719.7
useable range	$0 < \phi_n < 0.888$	$0 < \phi_n < 0.738$	$0 < \phi_n < 0.500$
maximum error	<3%	<0.9%	<0.02%

[a] Upper limit to the useable range is the maximum possible neutral surface volume fraction for each phase. The error quoted is the maximum error between the fitted and computed values of the mean curvature.

To determine $\langle K_n \rangle$ as a function of water volume fraction, it remains for us to find how the lattice parameter a varies with ϕ_n. We do this by noting that the total number of lipid molecules in the unit cell is given by multiplying the unit cell volume by the amphiphile volume fraction and then dividing by the volume of the amphiphilic molecule. Hence the area of the pivotal surface of one monolayer in the unit cell is given by

$$S_n = \frac{A_n}{2}\frac{a^3(1-\phi_w)}{\nu} \tag{17}$$

The Gaussian curvature as a function of ϕ_w is then

$$\langle K_n \rangle = \frac{2\pi\chi[A_n(1-\phi_w)/2\nu]^2}{[\sum_{i=0}\sigma_i((\nu_n/\nu)(1-\phi_w))^{2i}]^3} \tag{18}$$

Having determined the surface-averaged Gaussian curvature as a function of the water volume fraction it remains for us to do the same with the mean curvature. This is done by fitting computed values of the dimensionless mean curvature $H_n a$ to a series expansion in odd powers of ϕ_n.

$$H_n = \frac{\sum_{i=0}\varsigma_i\phi_n^{2i+1}}{a} = \frac{A_n\sum_{i=0}\varsigma_i[\nu_n/\nu(1-\phi_w)]^{2i+1}}{2\nu\sum_{i=0}\sigma_i[\nu_n/\nu(1-\phi_w)]^{2i}} \tag{19}$$

The values of ς_i for each bicontinuous cubic phase are given in Table 2.

Of course the frustration present in constant mean curvature interfaces is bound up in variations in amphiphipile chain extension. The variations in the monolayer thickness for constant mean curvature bicontinuous cubic phases have been described previously,[19] but unfortunately they have only been calculated for Q_{II}^D. In this case the variance in monolayer thickness has been computed to be

$$\langle l^2 \rangle - \langle l \rangle^2 = 3.5 \times 10^{-4}(1-\phi_w)^2 a^2 \tag{20}$$

There is no point in attempting to calculate the surface-averaged frustration energy, since similar expressions have not been determined for the other cubic phases. Nevertheless, as we will go on to show, the general behavior of the variance in monolayer thickness of (20) will provide us with a qualitative tool for interpreting phase transitions between the inverse bicontinuous cubics.

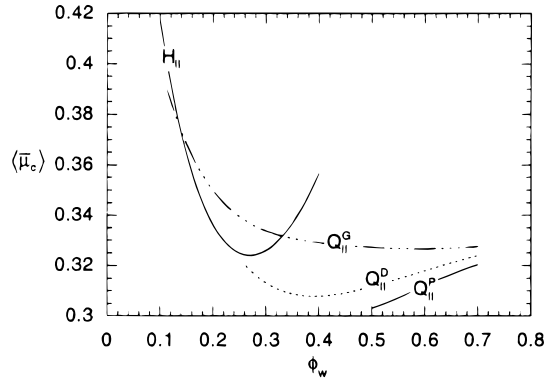

Figure 7. The curvature elastic energy for the constant mean curvature inverse bicontinuous cubic phases and the H_{II} phase for $A_n = 108$ Å^2, $\nu_n = 1230$ Å^3, $= 1736$ Å^3, $\bar{k}/k = 0.14$, and $H_r = -0.052$ Å^{-1}.

2.5. General Observations: Part II. The primary observation we make about the constant mean curvature geometry is that, except in the case where $\bar{k}/k = 1$, the energetic degeneracy in the curvature elasticity of the bicontinuous cubic phases is broken, Figure 7. Now the phase sequence $Q_{II}^G \rightarrow Q_{II}^D \rightarrow Q_{II}^P$, as one increases the water content, is set by the sequential reduction in free energy of each phase as well as their space filling properties. For the purposes of comparison we have plotted $\langle \bar{\mu}_c \rangle$ for the bicontinuous cubic phases and $\langle \bar{\mu}_c \rangle + \langle \bar{\mu}_f \rangle$ for the H_{II} phase using the same parameters as in Figure 6.

We are of course unable to plot $\langle \bar{\mu}_c \rangle + \langle \bar{\mu}_f \rangle$ for the cubics, because the variation in chain length extension for Q_{II}^G and Q_{II}^P and is unknown. However, a plot against water volume fraction for $\langle l^2 \rangle - \langle l \rangle$ makes the point that this variation is small, Figure 8, and we therefore assume that $\langle \bar{\mu}_f \rangle$ contributes only a small amount to the total free energy of the cubic phases.

Furthermore we make the observation that the physical frustration for a constant mean curvature bicontinuous cubic interface decreases as one increases the lipid volume fraction (i.e. it decreases as we dehydrate the system or heat it up). The physical frustration in the case of the parallel interface geometry acts in the reverse sense, increasing as one dehydrates or heats up. From this we draw the conclusion that when the water volume fraction is relatively great, the actual interfacial geometry is likely to be closer to a parallel interface and the energy of the Bonnet-related geometries will therefore approach degeneracy. When the water volume fraction is reduced the interfacial geometry will tend toward something closer to a constant mean curvature interface. Now the degeneracy is lifted.

The final observation we wish to make about this geometry is that there are well defined lower limits to the water volume fraction that each phase can sustain whilst retaining an interface

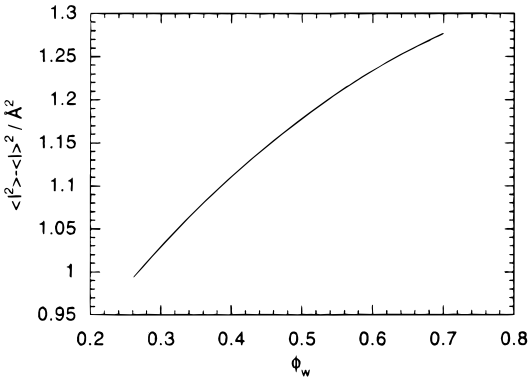

Figure 8. The variance in monolayer thickness for Q_{II}^D. The calculations were made for $A_n = 108$ Å^2, $\nu_n = 1230$ Å^3, and $\nu = 1736$ Å^3. The root mean square variation is of the order of 10% the average monolayer width.

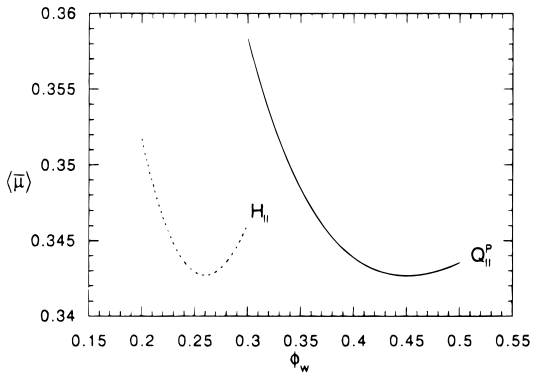

Figure 9. The value of $\bar{k}/k$ is determined by calculating the molecular free energies at which simultaneously phase coexistence occurs for the H_{II} and Q_{II}^P phases and where the equilibrium water compositions agree with the measurements made at 48 °C in 2:1 LA/DLPC. The conditions under which this occurs are $A_n = 108$ Å^2, $\nu_n = 1230$ Å^3, $\nu = 1736$ Å^3, $\bar{k}/k = 0.14$, $H_r = -0.054$ Å^{-1}, and $\eta/k = 0.001$ Å^{-2}.

with constant mean curvature.[17,18] Once again this is correlated with the space filling properies of each phase, with the minimum values of ϕ_w being 0.112, 0.262, and 0.500 for , Q_{II}^G, Q_{II}^D, and Q_{II}^P respectively. By way of contrast we calculate that the minimum water content for Q_{II}^P in the parallel interface geometry is 0.089. (This is the volume fraction at which the water channels on the cube face of Figure 1a close up.) So although low water contents might initally favor constant mean curvature monolayers over constant thickness ones, eventually the system must abandon this geometry if it wishes to dehydrate further. We will make use of this observation to make a qualitative explanation of the observed phase transition from Q_{II}^P to Q_{II}^D as temperature is raised in the C_{12} 2:1 FA/PC system.

3. Modeling the Experimental Results

Semiquantitative analysis of our results on 2:1 FA/PC mixtures must use the constant monolayer thickness geometry model of the inverse bicontinuous cubics, because of the lack of a calculated frustration energy for the constant mean curvature geometry. Hence our energetic model of the inverse hexagonal and bicontinuous cubic phases will depend on the three parameters, $\bar{k}/k$, H_r, and η/k.

We should be able to determine these parameters in the case of 2:1 LA/DLPC, since we have three quantities that we must fit: the excess water composition of the H_{II} phases; the excess water composition of the Q_{II}^P phase; and the fact that, at 48 °C, both phases are in energetic equilibrium, Figure 2a. The ratio $\bar{k}/k$ should not be a strong function of temperature. Using the chain calculations of Szleifer and co-workers,[20] we estimate that $1-(\bar{k}/k)$ should decrease in proportion to the square of the area at the pivotal surface, but not be a direct function of the temperature. At the resolution of our experiments[1] we are unable to detect a variation in between 30 and 49 °C and therefore we should not expect significant changes in $\bar{k}/k$. This observation allows us to use our determination of $\bar{k}/k$ as a reasonable estimate in all subsequent modeling, which will then only require us to know the mesophase composition at equilibrium in order to determine H_r and η/k.

3.1. Modeling the Effects of Water Composition and Temperature. Let us begin by considering the effects of water composition and temperature on 2:1 LA/DLPC, Figure 2a. The mesophase is destabilized at 48 °C at which point $\phi_w = 0.45$. The equilibrium volume fraction for the H_{II} phase at this temperature is approximately 0.26. Our measurements of the area neutral surface indicate that $A_n = 108$ Å^2, $\upsilon_n = 1230$ Å^3, and $\nu = 1736$ Å^3. It now remains for us to adjust our three material parameters in such a way as to obtain the correct equilibrium water volume fractions and ensure that the free energies of the two phases are equal, Figure 9. In so doing we find $\bar{k}/k = 0.14$, $H_r = -0.054$ Å^{-1}, and $\eta/k = 0.001$ Å^{-2} . The value of $\bar{k}/k = 0.14$ is in reasonable concordance with the value of 0.25 estimated from the equilibrium geometry of a highly swollen Q_{II}^P phase in a mixture of 1-monoolein, dioleoylphosphatidylcholine, and dioleoylphosphatidylethanolamine.[4] Furthermore both determinations agree with the theoretical prediction that $0 < \bar{k}/k < 1$.

Using $\bar{k}/k = 0.14$, we can now model the energetics of the bicontinuous cubic and hexagonal mesophases for the C_{12} mixture at 35 °C. We have adjusted the value of H_r in order to obtain an energetic minimum for the H_{II} phase at the experimentally determined value of $\phi_w = 0.27$, and have then adjusted η/k to obtain the correct equilibrium value of $\phi_w = 0.55$ for Q_{II}^P. This gives us $H_r = -0.052$ Å^{-1} and $\eta/k = 0.07$ Å^{-2}. The result is the free energy plot shown in Figure 6c.

For these values of the elastic parameters we of course obtain the correct phase ordering as we increase the water composition: $H_{II} \rightarrow Q_{II}^G \rightarrow Q_{II}^D \rightarrow Q_{II}^P$. A region of coexistence between H_{II} and Q_{II}^G is predicted, which by the common tangent construction should start at $\phi_w = 0.27$ and finish at $\phi_w = 0.47$. We do not observe this, because of the intervening lamellar phase, which we have not modeled here. Nevertheless the common tangent construction from our model predicts that if we had modelled the energy of the lamellar phase the coexistence region between L_α and Q_{II}^G would go up to at least $\phi_w = 0.47$. From our experimental work it appears that the limit to the region of coexistence is in fact $\phi_w = 0.42$.

The overextended region of coexistence between L_α and Q_{II}^G predicted by the model indicates that the H_{II} phase must probably be vertically displaced with respect to Q_{II}^G. This would occur if one altered the geometry of the bicontinuous cubic interfaces, Figure 7, and additionaly the energetic degeneracy would be broken.

It is very informative to calculate the relative contribution to the total free energy of the energy tied up in the physical frustration. According to our modeling of LA/DLPC at 35 °C, approximately 54% of the equilibrium free energy in the H_{II} phase is due to frustration, but only 1% of the total equilibrium free energy of the Q_{II}^P phase is accounted for in this way. In other words the energetic costs due to physical frustration are far more significant in the inverse hexagonal phase than those in the bicontinuous cubics.

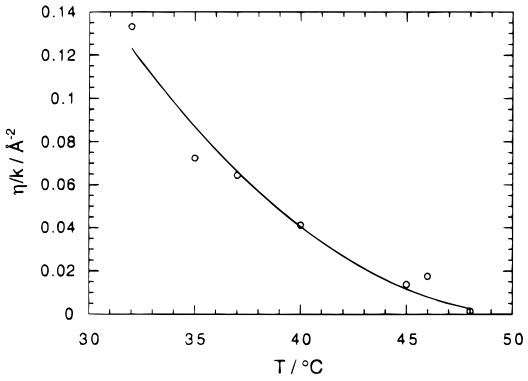

Figure 10. The calculated dependence of η/k on temperature for 2:1 LA/DLPC. A quadratic fit to the data is shown.

Even though at equilibrium the frustration energy in the bicontinuous cubic phases is of negligible magnitude with respect to the curvature elastic energy, the frustration energy has a significant effect on the equilibrium water composition. Without the presence of a frustration energy the equilibrium water volume fraction for Q_{II}^{P} would be 0.48 instead of 0.55. So despite its relatively small magnitude, the frustration energy can exert a profound influence on the swelling of the bicontinuous mesophases. The frustration energy always rises as the system is dehydrated since the inhomogeneity in molecular cross sectional area must necessarily rise as we increase the magnitude of the average mean curvature on a hyperbolic interface. The fact that, even though the frustration energy, is rather small compared to the curvature elastic energy it causes the system to swell by such a large amount, is due to the fact that the curvature elastic energy rises rather gently around the minimum in $\langle\bar{\mu}_c\rangle$, whereas the frustration energy rises steeply with decreasing water composition.

As we raise the temperature of the C_{12} system we observe a reduction in the lattice parameter of the bicontinuous cubic phases and their eventual destabilization, driven by changes in the preferred mean curvature and η/k. From our modeling, H_r actually changes by only 5%, while η/k is reduced by a factor of 49 for the same 13 °C temperature rise. In modeling the equilibrium behavior of the phases between 35 and 48 °C we find a linear variation of H_r with temperature given by

$$H_r(\text{Å}) = -0.0447 - 2.0 \times 10^{-4}\, T(°\text{C}) \qquad (21)$$

and a nonlinear variation in η/k, Figure 10, which over the same temperature interval is adequately modeled by

$$\frac{\eta}{k}(\text{Å}^{-2}) = 4 \times 10^{-4}\,(T(°\text{C}) - 51)^2 \qquad (22)$$

From (21) we find that the preferred value of the radius of curvature varies by approximately 0.09 Å °C^{-1}. This is comparable to the temperature variation in the *spontaneous radius of curvature* reported by Tate and Gruner[21] for DOPE of 0.1−0.2 Å °C^{-1}.

The variation in η/k with temperature appears to reside in variations in η. According to Szleifer and co-workers[20] k should decrease with area as $A_n^{-7.5}$, and should scale linearly with temperature. We are unable to detect a variation in A_n, but we can make a worst case estimate by assuming that the pivotal surface area has increased by an amount equal to the uncertainty in our measurements. Using this assumption, A_n would have increased from 108 to 110 Å^2 and according to the scaling laws k would be reduced by a factor of 0.9 for the 13 °C rise in temperature. In fact η/k has decreased by a factor of 49, which leads us to surmise that η has decreased by a factor of 54 over the same temperature interval. Therefore according to the model, the variation in the cubic unit cell size with temperature is predominantly driven by the rapid decrease in the packing frustration costs. The dehydration of the H_{II} phase on the other hand is driven by the smaller changes in H_r. This provides a possible rationalization for the characteristically greater decrease in lattice parameter with temperature observed in the bicontinuous cubic phases, when compared to the inverse hexagonal phase.

Because the water composition of the H_{II} phase is hardly altered, the frustration energy $\langle\bar{\mu}_f\rangle$ remains largely unchanged between 35 and 50 °C. In fact, at the equilibrium composition, it has increased by only $\langle\bar{\mu}_f\rangle = 0.002$ for this temperature rise. The frustration energy at equilibrium for the bicontinuous cubic has in fact decreased by $\langle\bar{\mu}_f\rangle = 0.003$. The destabilization of the bicontinuous cubic phase has arisen solely due to the greater increase in the curvature elastic energy cost, $\langle\bar{\mu}_c\rangle$, which is $\langle\bar{\mu}_c\rangle = 0.108$ for the cubic and only 0.019 for the H_{II} phase. The source of the additional curvature energetic cost in the bicontinuous cubic phases is in the negative Gaussian curvature of the saddle deformation and the associated inhomogeneity in the interfacial curvatures.

This indicates that, at least in this system, our conventional notions of increases in the magnitude of the preferred mean curvature driving the phase transitions may be correct.

Of course above 50 °C we continue to observe the D surface cubic in coexistence with the H_{II} phase. Our observations on the behavior of constant mean curvature cubic phases leads us to the following qualitative model of the Q_{II}^{P} to Q_{II}^{D} phase transition. At the high water volume fractions occuring at low temperatures the monolayer interface is approximately parallel to the underlying minimal surface. In this geometry, both the packing frustration and the curvature inhomogeneities are minimal, and the free energies of the cubic phases are degenerate. This agrees rather well with our observation of the relative stability of cubic phases in the region between 31 and 35 °C, Figure 2a. As the bicontinuous cubics dehydrate in response to increasing temperature, it becomes less and less likely that the interface will lie on a parallel surface, as both the curvature inhomogeneities and packing frustration increase rapidly, Figure 6b.

In situations, as here, where the magnitude of the mean interfacial curvature is rather small relative to the magnitude of the preferred mean curvature, the first half of the monolayer bending energetic, $(1 + \bar{k}/k)(H_n - H_r)^2$ will be the dominant term in the curvature elastic energy. The system may then tend toward an interface of constant mean interfacial curvature. Simultaneously, the packing frustration for the constant mean curvature interface will decrease and a net reduction in the free energy may become possible. The energetic degeneracy will as a consequence be broken. Where the systems is not yet too dehydrated, the most stable bicontinuous cubic phase will be Q_{II}^{P}. However, as we increase the temperature further the water composition of Q_{II}^{P} approaches its limiting value of $\phi_w = 0.5$. To dehydrate further the P cubic must move away from having constant mean curvature and hence suffer a steep rise in free energy with respect to the D surface cubic (compare the free energies of Figures 6c and 7).

It is interesting to observe that the phase transition from Q_{II}^{P} to $Q_{II}^{D} + H_{II}$ does indeed occur quite close to $\phi_w = 0.5$. Furthermore, the absence of the G surface cubic at higher

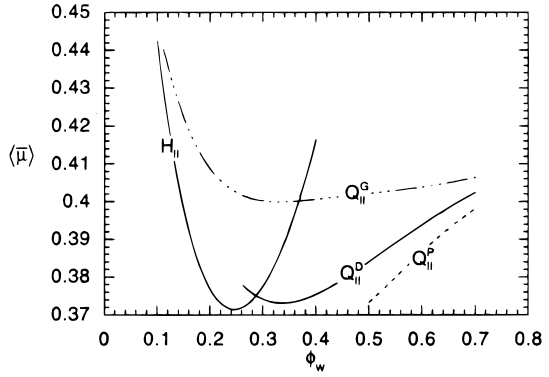

Figure 11. It is possible to simulate the phase transition in 2:1 LA/DLPC at 18 °C if we use the constant mean curvature model for the free energy of the cubic phases. The calculation has been made using $A_n = 108$ Å^2, $\nu_n = 1230$ Å^3, $\nu = 1736$ Å^3, $\bar{k}/k = 0.14$, and $H_r = -0.058$ Å^{-1}.

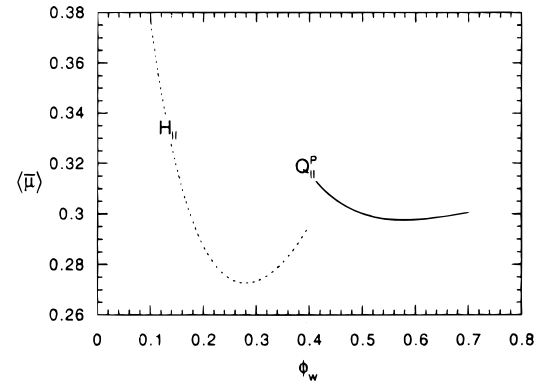

Figure 12. The calculated molecular free energy of the H_{II} and Q_{II}^P phases at 55 °C in 2:1 MA/DMPC are plotted as a function of water volume fraction for $A_n = 109$ Å^2, $\nu_n = 1453$ Å^3, $\nu = 1948$ Å^3, $\bar{k}/k = 0.125$, $H_r = -0.051$ Å^{-1} and $\eta/k = 0.12$ Å^{-2}.

temperatures can also be explained if the system has moved towards an interface of constant mean curvature, Figure 11.

3.2. Modeling the Effects of Chain Length. We now turn to an examination of the effect of increasing chain length on the stability of the bicontinuous cubic phases, by looking at the energetics of 2:1 MA/DMPC. Following the same procedure as before we have modelled the energetics in this system at 55 °C, Figure 12, where the equilibrium value of ϕ_w for the H_{II} phase is 0.28 and is 0.58 for the *Im*3*m* cubic. Using $A_n = 109$ Å^2, $= 1948$ Å^3, and $\nu_n = 1453$ Å^3 and scaling $\bar{k}/k$ to a new value of 0.16, since the ratio is proportional to A_n^2, we obtain $H_r = -0.050$ Å^{-1} and $\eta/k = 0.13$.

Experimentally we observe that increasing chain length destabilizes the bicontinuous cubic phases, but complete destabilization only occurs at C_{16} not C_{14}. The modelling indicates the correct trend for increasing chain length, but it has apparently overestimated the relative stability of the H_{II} phase. We recall that the same effect was responsible for the overestimate of the region of coexistence between between the L_α and Q_{II}^G phases in section 3.1.

The stabilization of the H_{II} phase with respect to the bicontinuous cubics as one increases chain length occurs because of the reduction in the packing frustration. In 2:1 LA/DLPC the frustration energy in the H_{II} phase is 54% of the total free energy per molecule, whereas in MA/DMPC it is proportionately smaller at 47% of the total. The packing frustration energy in the bicontinuous cubic phases has at the same time increased, but only from 1% to 2% of the total. According to this model, it is the reduction in the H_{II} phase frustration which is the dominant factor in destabilizing the cubics.

The reduction in the magnitude of H_r with increased chain length indicated by the modelling, while counter intuitive, is clearly implied by the increased hydration of the H_{II} phase. Previously we reasoned that the decrease in η/k with increasing temperature resulted in the dehydration of the cubic phases which would end up favoring Q_{II}^D over Q_{II}^P. This transition was observed as we raised the temperature in 2:1 LA/DLPC at $\phi_w = 0.45$. In the case of MA/DMPC the Q_{II}^P phase is destabilized at 70 °C when $\phi_w = 0.52$, but no Q_{II}^D phase is observed at higher temperatures. We find $\eta/k = 0.09$ and $H_r = -0.054$ Å^{-1} at this temperature. So the preferred mean curvature at the destabilisation temperature is the same as we found for LA/DLPC, but η/k is 90 times larger and the system is not as dehydrated. These data would suggest that there is a critical window in these parameters around $\phi_w = 0.5$, which must be achieved if one is to observe a Q_{II}^P to Q_{II}^D phase transition. In this case the Q_{II}^P phase does not dehydrate sufficiently to stabilize the D surface cubic.

4. Concluding Remarks

By constructing models based on the competition between curvature elastic and molecular packing costs for amphiphiles in the inverse hexagonal and inverse bicontinuous cubic phases, we have been able to model the phase behaviour of 2:1 FA/PC mixtures. Our findings indicate that the energetic costs of molecular packing frustration in the H_{II} phase is far greater than in the inverse bicontinuous cubics, but precisely the reverse is true for the curvature elastic costs. This means that the relative phase stability is governed by rather small variations in the differences of quite large quantities.

At short chain lengths the inverse bicontinuous cubic phases will be favored, because the packing costs of the H_{II} phase are high. This also means that the H_{II} phase will be found on the low water content side of the cubics. As we raise the temperature the desire for interfacial curvature increases, which raises the curvature elastic costs of the cubic phases sufficiently to stabilize the hexagonal phase. Increasing chain lengths of course reduces the packing costs in the H_{II} phase significantly and this acts to stabilize it with respect to the bicontinuous phases.

For the first time we have shown that the degeneracy of the inverse bicontinuous cubic phases is broken by changes in the geometry of the interface. For constant mean curvature interfaces this gives rise to the observed phase sequence with water content of $Q_{II}^G \rightarrow Q_{II}^D \rightarrow Q_{II}^P$. Our analysis of 2:1 FA/PC mixtures suggests that the destabilization of Q_{II}^P as we increase the temperature may be understood in terms of the requirement for the interface to alter geometry as it dehydrates from one of almost constant mean curvature to one which approaches a constant thickness monolayer.

Although we believe that our analyses form a useful basis for understanding the phase and structural behaviour of inverse lyotropic mesophases, we should point to some of the weaknesses in what we have done.

Our interpretation suffers, as have other models, from setting the interfacial geometry a priori, rather than allowing it to be governed by the energetic of the monolayer. The interesting results obtained with the constant mean curvature model of the inverse bicontinuous cubic phases points to this. Furthermore, the large (49-fold) change in η/k that is required to model the

dehydration of Q_{II}^{P} over a 13 °C interval is almost certainly not real, but an effect of having fixed the interfacial geometry in the model. We would surmise that in fact the interfacial geometry of these phases is moving away from being parallel to the underlying minimal surface as we raise the temperature and increase the interfacial curvature and that when more accurately modeled the over large variations in η/k will disappear, and that the phase transition from Q_{II}^{P} to Q_{II}^{D} will be observed. We have also not included energetic terms involving inter-bilayer forces or higher order curvature elastic moduli. Given that we have already seen that marginal variations in the molecular free energy of different mesophases trigger phase transitions, it is prudent to assume that an accurate theory of the phase transitions in these systems would need to include such terms. Whenever one is dealing with a system containing more than one lipid species it is of course possible that there may be component segregation. We have no experimental evidence for this in any of the data we have modeled. Furthermore even partial component segregation would be expected to have detectable structural effects in this system, since the fatty acids will form inverse micellar phases above the chain melting transition. We have no evidence for this.

Progress in our understanding of the phase behaviour of complex lyotropic systems such as these will rely on our ability to disentangle and model all the important energetic contributions to the molecular free energy. From the point of view of theoretical interpretation it seems clear from this work that further progress will only be made when we devise means of calculating the interfacial geometry from the molecular energetics. This is a nontrivial task. Experimentally there is a need for more detailed data. Specifically we need to make accurate measurements of the geometry and energy of the lyotropic mesophases as a function of hydration at different temperatures and pressures. The addition of alkane to such systems may be used to estimate the packing frustration energy calorimetrically and measure the energy of dehydration in the absence of this effect. This will be at least one step along the road to separating out energetic terms. Interestingly, calorimetric measurements of the packing frustration energy we have made on other systems confirm that there is very little packing frustration in the inverse bicontinuous cubic phases,[6] but the packing frustration is at least an order of magnitude greater for the H_{II} phase, in agreement with the calculations shown here.

These observations and our modelling of 2:1 FA/PC mixtures all tend to confirm that the relative phase stability of the inverse hexagonal and bicontinuous cubic phases relies on the frustrated competition between homogeneous curvature and uniform molecular packing. Such competition can only occur when the ratio $\bar{k}/k$ lies between nought and one, in agreement with our estimate of $\bar{k}/k = 0.14$.

Acknowledgment. This work was funded in part by the EPSRC (Grant GR/K21054, GR/H10672 and GR/L48065), the Royal Society, and a British Council-DAAD grant. P. M. Duesing acknowledges the support of Unilever plc.

References and Notes

(1) Templer, R. H.; Seddon, J. M.; Warrender, N. A.; Syrykh, A.; Huang, Z.; Winter, R.; Erbes, J. *J. Phys. Chem. B* **1998**, submitted for publication.

(2) Seddon, J. M.; Templer, R. H.; Warrender, N. A.; Huang, Z.; Levc, G.; Marsh, D. *Biochim. Biophys. Acta* **1997**, *1327*, 131−147.

(3) Duesing, P. M.; Templer, R. H.; Seddon, J. M. *Langmuir* **1997**, *13*, 351−359.

(4) Templer, R. H.; Khoo, B. J.; Seddon, J. M. *Langmuir* **1998**, in preparation.

(5) Helfrich, W. *Z. Naturforsch.* **1973**, *28c*, 693.

(6) Khoo, B. J. Ph.D. Thesis, Imperial College, London, 1996.

(7) Templer, R. H. *Langmuir* **1995**, *11*, 334.

(8) Turner, D. C.; Gruner, S. M.; Huang, J. S. *Biochemistry* **1992**, *31*, 1356−1363.

(9) Duesing, P. M. Ph.D. thesis, Imperial College, London, 1995.

(10) Hyde, S. T. *J. Phys. Chem.* **1989**, *93*, 1458−1464.

(11) Helfrich, W.; Rennschuh, H. *J. Phys.* **1990**, *51*, C7189−C7195.

(12) Turner, D. C.; Wang, Z. G.; Gruner, S. M.; Mannock, D. A.; McElhaney, R. N. *J. Phys. II* **1992**, *2*, 2039−2063.

(13) Strom, P.; Anderson, D. M. *Langmuir* **1992**, *8*, 691−709.

(14) Templer, R. H.; Turner, D. C.; Harper, P.; Seddon, J. M. *J. Phys. II* **1995**, *5*, 1053−1065.

(15) Templer, R. H.; Seddon, J. M.; Warrender, N. A. *Biophys. Chem.* **1994**, *49*, 1−12.

(16) Kozlov, M. M.; Winterhalter, M. *J. Phys. II (France)* **1991**, *1*, 1077.

(17) Anderson, D. M.; Davis, H. T.; Scriven, L. E.; Nitsche, J. C. C. *Adv. Chem. Phys.* **1990**, *77*, 337−396.

(18) Grosse-Brauckmann, K. *J. Colloid Interface Sci.* **1997**, *187*, 418−428.

(19) Anderson, D. M.; Gruner, S. M.; Leibler, S. *Proc. Natl. Acad. Sci. U.S.A.* **1988**, *85*, 5364−5368.

(20) Szleifer, I.; Kramer, D.; Benshaul, A.; Gelbart, W. M.; Safran, S. A. *J. Chem. Phys.* **1990**, *92*, 6800−6817.

(21) Tate, M. W.; Gruner, S. M. *Biochemistry* **1989**, *28*, 4245−53.